Electronic origin of the anomalous stability of Fe-rich bcc Fe-Cr alloys

P. Olsson,[1] I. A. Abrikosov,[2] and J. Wallenius[3,4]
[1]*Departément Matériaux et Mécanique des Composants, Electricité de France, Les Renardières, F-77250 Moret-sur-Loing, France*
[2]*Department of Physics, Chemistry and Biology (IFM), Linköping University, SE-58183 Linköping, Sweden*
[3]*Department of Nuclear and Reactor Physics, Royal Institute of Technology, Stockholm, Sweden*
[4]*Department of Neutron Research, Uppsala University, Uppsala, Sweden*
(Received 26 September 2005; revised manuscript received 12 January 2006; published 14 March 2006)

The binary Fe-Cr alloy is a system with a miscibility gap. The decomposition occurs either via the nucleation and growth mechanism or as spinodal decomposition, depending on the Cr content. However, at low chromium concentrations the alloys are anomalously stable. This is shown to be true only for the *ferromagnetic* body centered cubic (bcc) phase. The stability stems from the negative mixing enthalpy at low concentrations of chromium. We show that the effect has an electronic origin, that is, it is directly related to variations of the electronic structure in the alloy with concentration. We also demonstrate that the variation in the state density of the majority channel at the Fermi level in the concentration interval below 20 at. % Cr indicates increasing tendency of the system towards the spinodal decomposition in the system. Moreover, in the equimolar concentration region, significant deviations of the spin up band from its canonical shape are observed, which destabilize the bcc phase.

DOI: 10.1103/PhysRevB.73.104416 PACS number(s): 75.50.Bb, 71.20.Be, 71.15.Mb

I. INTRODUCTION

The binary body centered cubic (bcc) Fe-Cr alloy is the base of many important industrial steels, especially in the nuclear industry. A moderate amount of Cr, up to 10%, has proven to be most beneficial when it comes to the ductile to brittle transition temperature[1] as well as corrosion resistance and resistance to neutron radiation induced swelling.[2–4] The equilibrium phase diagram for the Fe-Cr system[5] indicates the presence of the miscibility gap for the alloy concentrations above 10 at. % Cr at room temperature where a Cr-rich bcc α'-phase with up to 85 at. % Cr is precipitated. Previous studies[6–9] also demonstrated that there was a tendency towards clustering in bcc alloys with 10–85 at. % Cr. For lower concentrations of Cr the alloy is fully miscible, and moreover, diffuse-neutron-scattering experiments show a dramatic change of the ordering tendency towards the short-range order for these alloys.[6]

The anomalous stability of the bcc Fe-Cr alloys at low chromium concentrations can in fact be predicted from the band filling arguments. Indeed, it was demonstrated earlier[10] that ordered phases ought to be expected for alloys of transition metals with half-filled bands whereas phase separation would occur in alloys of transition metals with almost filled or almost empty bands, with a crossover point in the region of electron concentrations of interest. Similar conclusion was obtained in model calculations based on the generalized perturbation method (GPM).[11,12] Of course, the situation is complicated by the presence of the magnetism. But using the GPM model Hennion[13] has demonstrated that, indeed, the effective interatomic potential between the nearest neighbors varies with concentration in ferromagnetic bcc Fe-Cr alloys, and even changes sign at around 25 at. % Cr. Thus, mixing should decrease the total energy of dilute Fe-based alloys, while the clustering should be energetically preferable at higher Cr concentrations. From these simple arguments one can also expect that the mixing energy for bcc Fe-Cr changes sign as a function of alloy composition making low-Cr steels particularly stable.

However, earlier first-principles calculations[14] did not observe this effect. Also, the experimental mixing enthalpy in this system is positive everywhere, and exhibits regular solid solution behavior.[5] In a recent study of thermodynamic properties of Fe-Cr alloys, Olsson *et al.*[15] solved the problem. The authors demonstrated that the regular solid solution behavior is characteristic for the paramagnetic bcc Fe-Cr alloys simulated in Ref. 15 by the disordered local moment model.[16] At the same time, the mixing energy for ferromagnetic bcc alloys changes sign at about 10 at. % Cr, and the negative sign is predicted for the dilute Fe-based alloys. The failure of the earlier ferromagnetic calculations[14] to resolve the effect can most probably be attributed to the use of the supercells with high Cr concentrations to model the disorder effects, a suggestion which is confirmed by the resent studies of Jiang *et al.*[17]

In this work, two different approaches have been used in order to calculate the variation of the mixing enthalpy in Fe-Cr alloys. Firstly, we used the effective medium approach represented by the exact muffin-tin orbitals theory within the coherent potential approximation (EMTO-CPA).[18] The same method was used in Ref. 15. Secondly, we employed the supercell approach and the projector augmented wave (PAW) method[19] implemented in the Vienna *ab initio* simulation package (VASP).[20–22] Both techniques predict similar behavior of the mixing enthalpy with well-defined minimum for Fe-rich alloys, if somewhat different in strength. We also present a detailed analysis of the electronic structure of bcc Fe-Cr alloys, and show that the stability of alloys with low Cr concentration has an electronic origin.

II. METHODOLOGICAL BACKGROUND

The calculations were performed in the framework of density functional theory (DFT).[23] In this study the general-

ized gradient approximation (GGA)[24] for the one-electron potential and the total energy was used as it is known that the local density approximation predicts the wrong ground state for iron.

A. Effective medium approach

The wave functions were expanded using a basis set of exact muffin-tin orbitals.[25–27] The Green's function technique was used in two steps in order to solve the one-electron problem.[28] First the iteration towards self-consistency was performed with overlapping potential spheres that cover the entire space. Then this approximation was corrected for by using the full charge density method.[29] The reliability of this combined technique is justified by the variational properties of the total energy functional. The accuracy has also been demonstrated in practice.[29]

Substitutional disorder was treated using the coherent potential approximation (CPA)[18,30–32] which provides reliable electronic structure and total energies for completely random alloys,[33,34] especially in the case of alloys where the constituents are of similar size. The method is based on a single-site approximation and has the advantage of speed and full flexibility of choice in alloy composition. The Fe-Cr system has previously been studied using the CPA by Turchi *et al.*[12] in the nonmagnetic case, as well as by Kulikov and Demangeat[35] in the ferromagnetic (FM) case. Akai and Dederichs[16] showed that there is a strong influence of magnetism in Fe-Cr, especially in the difference between a ferromagnetic alloy and an alloy where the magnetic moments randomly point "up" or "down," the so-called disordered local moments (DLM) model. It simulates the fully random paramagnetic (PM) Fe-Cr alloy, which can be written as a quaternary alloy $(\mathrm{Fe}\uparrow\text{-}\mathrm{Fe}\downarrow)_{1-c}(\mathrm{Cr}\uparrow\text{-}\mathrm{Cr}\downarrow)_c$ within this approximation.

A basis set of s, p, d, and f orbitals was used. Special attention was devoted to the region of low chromium concentration. The equations of state were calculated with a concentration increment of 1% between 0% and 10 at. % Cr and with an increment of 5% for the remaining compositions. 1240 k points in the irreducible part of the Brillouin zone were used and the self-consistent calculations were converged to the order of 10^{-5} eV. The calculations were spin-polarized, and we considered either ferromagnetic or DLM spin configurations. In our EMTO-CPA calculations the volume of the underlying bcc lattice was relaxed, but local ionic displacements off the sites of the bcc lattice were not taken into account.

B. Supercell method

The projector augmented wave (PAW) method[19] implemented in the Vienna *ab initio* simulation package (VASP)[20–22] was used in order to study supercells. The PAW method is a full potential method which Jiang *et al.*[17] used in a study of the Fe-Cr system using special quasirandom structures (SQS) with 16 atoms. A study of the magnetic moments of Cr atoms in ferromagnetic Fe-Cr alloys with this technique has also been done by Mirzoev *et al.*[36] Hafner *et al.*[37] studied the magnetic ground state of Cr by means of the VASP implementation of the PAW method. The method allows us to take the local effects into account but is limited in compositional flexibility.

The calculations within the PAW-SQS scheme were spin-polarized and fully relaxed using both ionic and volume relaxations. Sampling of the 27 k points was done according to the algorithm of Monkhorst and Pack.[38] It has previously been shown that the energies are well converged with respect to k points in similar cases.[39,40] The substitutional disorder was treated by creating special quasirandom structures,[41] which are supercells at the bcc underlying lattice. In this work we constructed several 128-atom SQS using the technique developed by Simak.[42] The large number of atoms is required in order to minimize the short-range order parameters for the lower concentrations and was used consistently for all calculations. SQS with 3.125, 6.25, 12.5, 25, 50, 75, and 96.875 at. % Cr were constructed.

III. EXPERIMENTAL BACKGROUND: PHASES AND MAGNETISM

From the phase diagram[5] of the Fe-Cr alloy we know that iron has three solid phases under normal pressure: bcc (α), fcc (γ), and bcc (δ) in the order of increasing temperature. The α-Fe is ferromagnetic (FM-α) or paramagnetic (PM-α), depending on the temperature, the high-temperature γ-Fe is paramagnetic, though it is supposed to be antiferromagnetic at $T=0$ K. In the alloy two more interesting solid phases occur: the paramagnetic α' phase and the structurally complex σ phase. The α' phase coexists with the α in the concentration range of about 10–85% Cr below 475 °C. α' is a chromium-rich phase which appears either in nucleation (for around 10 at. % Cr) or spinodal decomposition (above about 20 at. % Cr). The σ phase appears around equimolar concentrations and is a tetrahedral close-packed structure with 30 atoms distributed on five special positions of space group 136 (D_{4h}^{14}, $P4_2/mnm$). Recently, Korzhavyi *et al.*[43] carried out a study of site occupancy and stability of the σ phase, and analyzed it in great detail. We therefore will not further discuss the σ phase in this work. Also, we note that the magnetic structure is rather complex for Cr and Cr-rich alloys,[44,45] and the total energy of pure Cr is lowered by a magnetic contribution, estimated to be between 7 and 46 meV.[17,37] However, the Néel temperature for Cr is relatively low, 311 K, and therefore it is appropriate to treat Cr as nonmagnetic at temperatures of interest for steel applications in the power industry.

IV. RESULTS AND DISCUSSION

A. Lattice parameters and local lattice relaxations

We first investigate the concentration dependence of the lattice parameter for bcc Fe-Cr alloys, as well as the magnitude of the local displacement of ions off the sites of the average underlaying bcc lattice. Figure 1 displays the calculated lattice parameters for FM and DLM Fe-Cr alloys, as well as the measurements in the ferromagnetic bcc phase from the literature.[46] The measured ferromagnetic lattice parameter exhibits a small deviation from linearity, which is

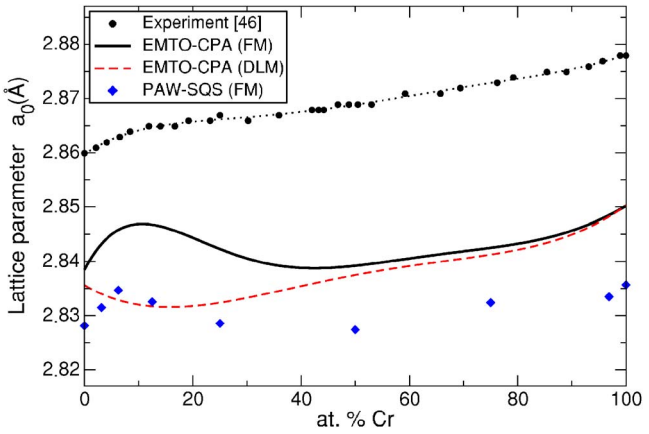

FIG. 1. (Color online) Lattice parameters of the bcc Fe-Cr alloys as a function of Cr concentration. EMTO-CPA data for the ferromagnetic phase (FM, solid line) and disordered local moment phase (DLM, dashed line) as well as PAW-SQS data for the ferromagnetic alloys (diamonds) are presented. The measured ferromagnetic data (circles) are taken from Ref. 46.

strongest in the region of low chromium content. Both the ferromagnetic CPA and the SQS calculations exhibit the same variation, although somewhat exaggerated. At 10 at. % Cr, both methods predict a local maximum in the lattice parameter of the ferromagnetic phase, with values close to the corresponding value for pure Cr. The lattice parameters predicted by the EMTO-CPA and PAW-SQS methods differ by an almost constant 0.01 Å for all concentrations. It thus seems to be a difference purely related to the EMTO and PAW formalisms and not to the method of representing disorder. For comparison we also show the results of the DLM calculations, which exhibit a small deviation from linearity in the opposite direction, as compared to the ferromagnetic calculations. In general, we find the agreement between theory and experiment satisfactory. The theoretical lattice parameters are slightly underestimated, by less than 1%, which is typical accuracy for GGA calculations. Thus, in our simulations of the mixing energy we can safely use theoretical lattice parameters.

Note that the data presented in Fig. 1 show the lattice parameter for the average bcc lattice. At the same time, the individual bond lengths can vary due to the effect of the local lattice relaxations. As a matter of fact, Jiang *et al.*[17] observed remarkable dispersion of the static ionic displacements in Fe-Cr alloys, even though the alloy components are almost perfectly size matched.[47] However, the results are obtained for relatively small SQS. Here we would like to point out that the convergence of the results as a function of the SQS size can depend on the physical property studied with these SQS.[48] For example, the total energy usually converges relatively fast, and small SQS are often sufficient for its accurate estimate. On the other hand, the density of states calculated with small SQS sometimes exhibit quite a sharp peak structure[49,50] that disappears with increasing supercell size.[33] Here we check conclusions made in Ref. 17 by calculating individual bond lengths in 128-atom SQS by PAW-VASP. Also, it is important to estimate the contribution to the alloy energetics due to local lattice relaxations.

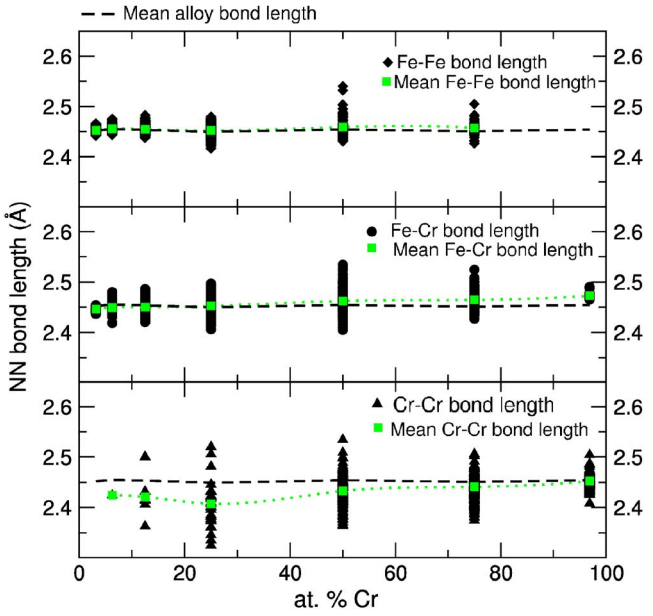

FIG. 2. (Color online) Pair bond lengths for 128-atom SQS supercells in fully relaxed PAW calculations with alloy concentrations ranging from 3.185–96.875 at. % Cr. The top panel displays the individual bond lengths between Fe-Fe pairs (diamonds) and the mean Fe-Fe bond length (squares) for the given concentrations. The middle panel displays the individual bond lengths between Fe-Cr pairs (circles) and the mean Fe-Cr bond length (squares) for the given concentrations. The bottom panel displays the individual bond lengths between Cr-Cr pairs (triangles) and the mean Cr-Cr bond length (squares) for the given concentrations. The concentration dependence of the mean alloy bond length is indicated in all panels as a dashed line.

In agreement with Jiang *et al.*,[17] we find that local lattice relaxations are indeed significant in magnitude. Figure 2 displays the scattering of the pair bond lengths for Fe-Fe, Fe-Cr, and Cr-Cr pairs for alloys with different compositions. The pair bond lengths diverge maximally 4% from the alloy mean value. Although the local relaxations are significant, the calculated mixing energy, which is discussed in detail below, does not change by more than 8% at equimolar concentration as compared to the unrelaxed case. However, local relaxations are crucial for the PAW calculations since they do give rise to the negative mixing enthalpy for alloys with low Cr concentration. Still, in absolute values the difference is of the order of 5 meV in this concentration interval. Therefore, we conclude that the neglect of the local lattice relaxations in the EMTO-CPA calculations for random Fe-Cr alloy is fully justified.

B. Mixing enthalpy

The mixing enthalpy H of an alloy with x parts Cr is defined as

$$H(\mathrm{Fe}_{1-x}\mathrm{Cr}_x) = E(\mathrm{Fe}_{1-x}\mathrm{Cr}_x) - (1-x)E^{\mathrm{st}}_{\mathrm{Fe}} - xE^{\mathrm{st}}_{\mathrm{Cr}}, \qquad (1)$$

where all total energies E are calculated at corresponding equilibrium volumes, and the two last terms represent the

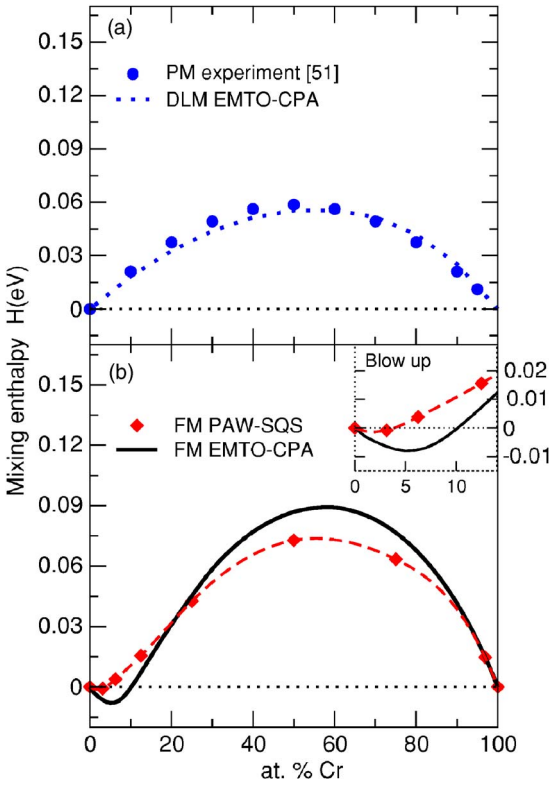

FIG. 3. (Color online) (a) Concentration dependence of the mixing enthalpy of disordered DLM bcc Fe-Cr alloys from 0–100% Cr, as predicted by the EMTO-CPA method (dotted line), in comparison to measurements for the paramagnetic alloys[51] (circles). (b) Concentration dependences of the mixing enthalpy for disordered FM bcc Fe-Cr alloys from 0–100% Cr, as predicted by the EMTO-CPA (solid line) and PAW-SQS (diamonds) methods. Inset in (b) is a blow up of the Fe-rich region with 0–14 at. % Cr to better show the predicted change in sign of the mixing enthalpy in the FM alloys.

energies of the standard states for pure Fe and Cr, respectively.

The experimental information for the mixing enthalpy of random bcc Fe-Cr alloys is available only at high temperature (T=1600 K),[51] where the alloys are paramagnetic. In order to simulate the effect of magnetic disorder we calculated $E(Fe_{1-x}Cr_x)$ using the EMTO-CPA technique and the DLM model. As standard states we have chosen DLM bcc Fe and nonmagnetic bcc Cr. Our results are shown in Fig. 3(a). Note that the DLM mixing enthalpy, which in Fig. 3(a) is compared to measured data,[51] agrees well with the experiment and does not exhibit any nonmonotonous variation.

The calculated mixing enthalpy of the ferromagnetic Fe-Cr alloy is shown in Fig. 3(b). As standard states we used FM bcc Fe and nonmagnetic bcc Cr. Here we would like to mention once again that the validity of the Cr-rich side of our curve is somewhat more questionable than the Fe-rich side since the reference state is paramagnetic Cr rather than the incommensurate magnetic spin-density wave state that is the true ground state for Cr.[44,45] Note, that to this day, density functional theory fails to correctly predict the ground state for Cr.[37,52] However, as was mentioned earlier in Sec. III, we believe that our model is appropriate for the temperatures of interest for steel applications in the power industry because of the low Néel temperature of Cr.

In Fig. 3(b) one can clearly see that the mixing enthalpy of ferromagnetic bcc Fe-Cr alloys has a well-defined minimum for low concentrations of Cr. Although the depth and width of the minimum differs for PAW-SQS and EMTO-CPA calculations, the trend is clearly similar in both the supercell and the effective medium simulations. The negative sign of H clearly indicates the ordering tendency in the system that stabilizes the alloys against the phase separation that occurs at higher Cr concentrations, and explains the anomalous stability of Fe-Cr observed on the iron side of the alloy phase diagram.

C. Electronic structure and the phase stability

In order to explain the variation of the mixing enthalpy of the ferromagnetic bcc Fe-Cr alloys as a function of concentration we study their electronic density of states (DOS). Because of the good qualitative agreement between the EMTO-CPA and PAW-SQS results for the mixing enthalpies seen in Fig. 3(b), we calculate the DOS using the numerically more efficient EMTO-CPA method. The electronic structure of random Fe-Cr alloys has been studied earlier within the CPA by Kulikov and Demangeat[35] and with the augmented space recursion method by Ghosh *et al.*,[53] but with the aim to understand the magnetic properties of the alloys. Here we will concentrate on the phase stability aspects of the problem.

In Fig. 4 the density of states for bcc ferromagnetic Fe-Cr alloys is plotted. The DOS curves are plotted with an increment of 2% from pure iron to the $Fe_{0.90}Cr_{0.10}$ disordered alloy and then with an increment of 10% up to pure chromium. Starting with pure Fe and pure Cr, we see that their DOS has canonical shapes characteristic for the bcc transition metals with two well-defined regions corresponding to the bonding (low energy peaks) and antibonding (high energy peaks) states separated by a pseudogap. The pseudogap minima in both spin channels are indicated with dashed lines in Fig. 4. For Cr, the bonding states are almost completely filled while the antibonding states are empty for both spin channels, which explains the very high stability of bcc Cr. For Fe, the majority spin channel is almost fully saturated, and therefore it contributes very little to the cohesion of the crystal. But for the minority spin band the situation is very similar to Cr, with filled bonding and empty antibonding states. Thus, bcc Fe is also quite stable. Upon alloying of Fe with Cr both the electron concentration and magnetic moment (see Fig. 5) decrease. The most energetically favorable way for the Fe-Cr system to achieve this is, according to our first-principles calculations, to keep the Fermi energy pinned by the pseudogap of the minority spin band (see dashed line in Fig. 4) while depopulating the antibonding states of the majority spin band.

In fact, it is clearly seen in Fig. 4 that almost all the variation of the DOS appear in the spin-up band. For alloys with high (>10%) concentration of Cr, the majority spin states are gradually forced through the Fermi level. However, because of the high peak of the spin-up DOS that has to pass the Fermi level, the energetics of the transition is unfavor-

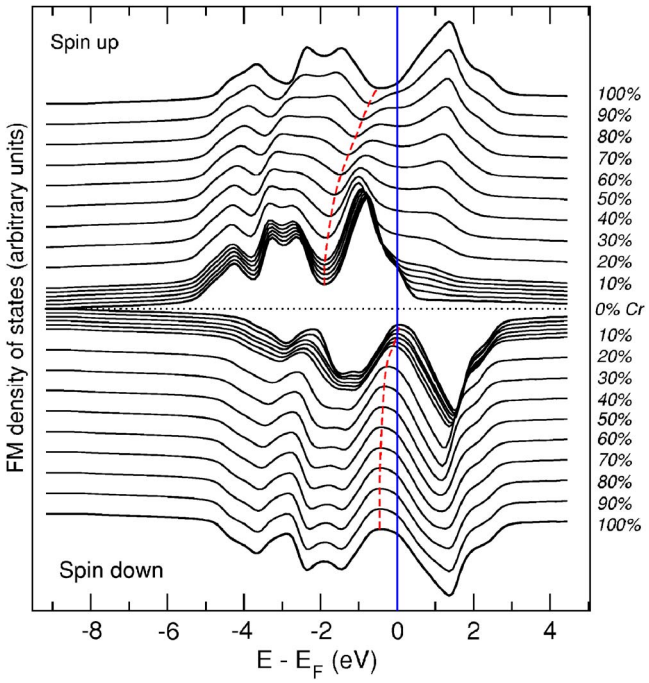

FIG. 4. (Color online) Average total density of states for the FM Fe-Cr alloy from 0–100% Cr, as predicted by the EMTO-CPA method. The spin-up states are displayed above the abscissa and the spin-down states below. The DOS are shifted along the ordinate axis proportionally to their Cr content. The pseudogap minima in both the spin-up and spin-down channels are traced by dashed lines. The vertical line marks the Fermi energy.

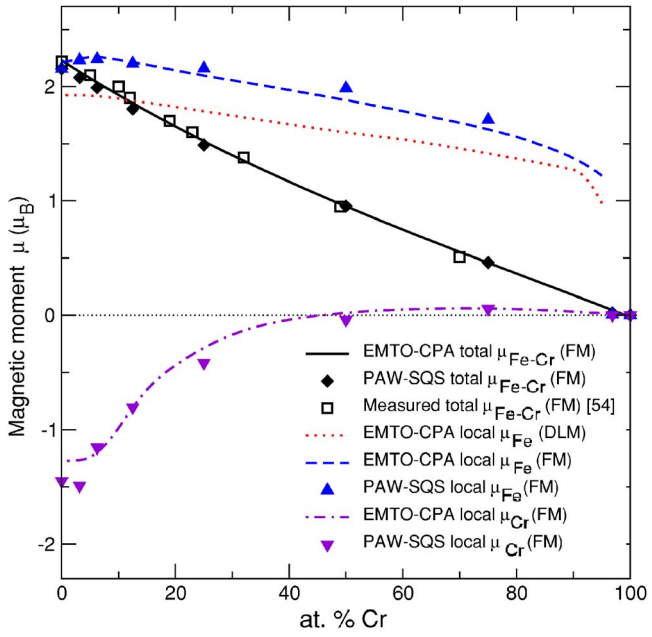

FIG. 5. (Color online) Concentration dependences of the net and local magnetic moments in Fe-Cr system. EMTO-CPA predictions of the total net magnetic moments for the FM samples (solid line), as well as average local Fe (dashed line) and Cr (dashed-dotted line) moments in the FM state are shown. Average DLM moments at Fe atoms are given by the dotted line. Results of the PAW-SQS calculations of the total net moments (diamonds), average local Fe (triangles △), and average local Cr moments (triangles ▽) for the FM supercells are also shown in the figure. The measured (Ref. 54) net FM moment (squares) is included for comparison.

able, leading to the positive sign of the mixing enthalpy for most of the alloy concentrations. The energy cost of this electronic transition is illuminated by the fact that as it takes place the structure of the spin-up DOS curve loses its canonical shape, and around equiatomic composition the band is almost completely smeared out. Though the electron occupancy at the Fermi level remains at a more or less constant value, the value itself is relatively high, and may provide an opportunity for another structure, such as the mixture of the α and α' phases or the σ phase, to compete with the single-phase bcc solid solution.

However, at Cr concentrations below 10 at. % the situation is somewhat different. In Fig. 4 it is clearly seen that the band deformation effect is present also in dilute alloys. Indeed, the antibonding spin-up states are depopulated, and the mechanism of this depopulation is associated with a transfer of the spectral weight from the states just below the Fermi energy to the states about 1 eV above E_F, giving rise to a formation of a peak which at even higher concentrations is developing into the antibonding peak of pure Cr. At the same time, the behavior of the remaining part of the majority spin band in Fe-rich alloys with very small Cr concentration is still quite stiff, as shown in Fig. 4, and in more details in Fig. 6. The most pronounced modification of the band structure is associated with a shift of the tall antibonding peak towards the more negative energies with respect to the Fermi energy (see Fig. 4). Such a shift should decrease the one-electron energy of the system. As a matter of fact, the situation is similar to what was discussed by Jones[55,56] who showed that a relative stability of an alloy phase is enhanced if its density of states curve involves a large peak and a subsequently rapidly declining slope. Also, one can notice that in the same interval of concentrations, the Fermi level in the spin-down channel (see dashed line in Fig. 4) is progressing through the pseudogap minimum. While the latter effect is smaller than the former, both are energetically favorable, and compete with the energy lost due to the band deformation. According to our total energy calculations, the net effect is the energy gain in random alloys, which leads to the anomalous stability of the bcc Fe-Cr alloys at low concentrations of chromium.

D. Electronic structure and the spinodal decomposition

Above about 20 at. % Cr the α' Cr-rich phase appears via the spinodal decomposition of the bcc solid solution, that is, it appears spontaneously and without any energy barrier. In general, the mode of a structural decomposition is determined by the curvature of the free energy, $G=H-TS$. For positive curvatures any segregation occurs as nucleation and growth, while for negative curvatures the segregation is spinodal, forming interconnected Cr rich regions in the bulk.

Considering $T=0$ K, and in the simplest formulation of the rigid band model, the band structure contribution H_{bs} to the second derivative of the mixing enthalpy d^2H_{bs}/dc^2 is inversely proportional to the DOS at the Fermi level[55,57–59]

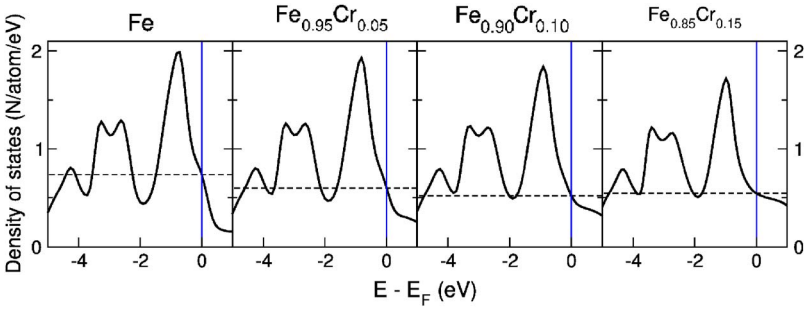

FIG. 6. (Color online) Density of states for the spin up channel for alloys with concentrations ranging from 0–15 at. % Cr. The vertical line marks the Fermi level, and the horizontal dashed line indicates the DOS at the Fermi energy for the corresponding alloy concentration.

$$\frac{d^2H_{\mathrm{bs}}}{dc^2} = \frac{(Z_{\mathrm{Cr}} - Z_{\mathrm{Fe}})^2}{n(\epsilon_F)}, \tag{2}$$

where Z_{Fe} and Z_{Cr} are the valence numbers of the alloy components. Of course, the sign of this derivative is always positive within the rigid band model, so the spinodal decomposition would never occur. Thus, the sign change of the second derivative of the mixing enthalpy, obtained in our first-principles calculations (see Fig. 7) is associated with deviations of the electronic structure in Fe-Cr system from the rigid band behavior, as was discussed in the previous section. At the same time, a correlation between d^2H_{bs}/dc^2 and the DOS at the Fermi level, which follows from Eq. (2) is observed in other systems with the spinodal decomposition.[57,58] Thus, an upturn on the concentration dependence of the DOS at E_F (see Figs. 6 and 7) indicates an increasing tendency of the system towards the spinodal decomposition.

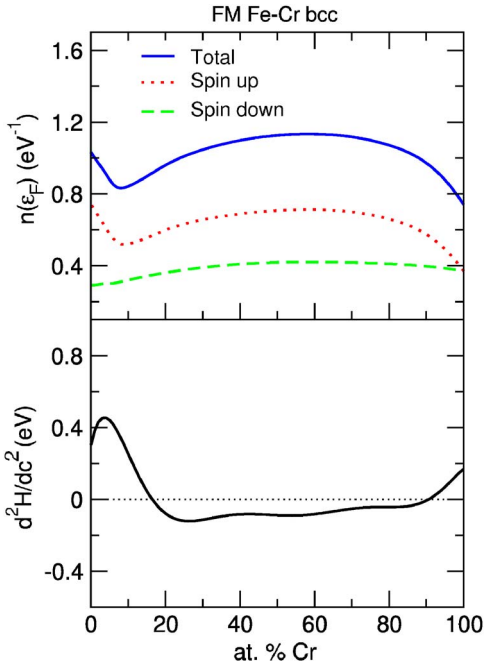

FIG. 7. (Color online) Top panel: The concentration dependence of the density of states at the Fermi level $n(\epsilon_F)$. Total DOS is indicated with a solid line, while the contributions from spin-up and spin-down channels are given by dotted and dashed lines, respectively. Bottom panel: The concentration dependence of the curvature of the mixing enthalpy.

The DOS at the Fermi level and the second derivative of the mixing enthalpy are plotted against the Cr concentration in Fig. 7. Similar to Refs. 57 and 58, one can clearly see the anticorrelation in the behavior of the DOS and d^2H_{bs}/dc^2. In its own turn, this means that the spinodal decomposition in Fe-Cr system has an electronic origin, namely it is directly related to variations of the electronic structure in the alloy with concentration. Moreover, it is determined by the majority spin electrons. Indeed, variations of the minority spin DOS at the Fermi level are rather uniform for all concentrations. Note that the second derivative of the mixing enthalpy changes sign at 16 at. % Cr. Neglecting the concentration dependence of vibrational and magnetic entropy, the predicted limit for spinodal decomposition is at this concentration, which is in excellent agreement with recent Mössbauer spectroscopy measurements.[60]

E. Electronic structure of alloys with local moment disorder

The DOS for the DLM Fe-Cr alloys are presented in Fig. 8. Since both spin states are identical, only one of them is

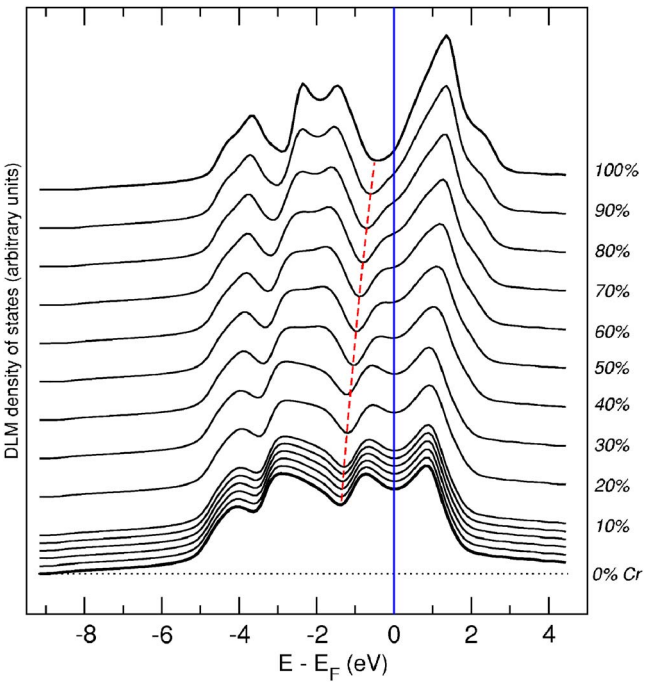

FIG. 8. (Color online) Average total density of states for the DLM Fe-Cr alloy from 0–100% Cr, as predicted by the EMTO-CPA method. Notations are the same as in Fig. 4.

plotted. For the iron rich alloys, the Fermi level cuts through the minority band, giving rise to a higher energy in comparison to the FM case where the number of occupied states at the Fermi level is small. As the electron occupancy is decreased, the pseudogap comes closer to the Fermi level and the differences between the DLM alloys and the FM alloys decrease, as can be seen in Figs. 3 and 1.

As seen in the figures above, magnetism is very important in order to understand the properties of the alloy. The total and local magnetic moments calculated by EMTO-CPA and PAW-SQS are plotted in Fig. 5. No significant difference in the alloy moments is found between the predictions of the EMTO-CPA and the PAW-SQS methods and theory agrees well with experiment.[54] The local iron moment in the DLM alloy (EMTO-CPA calculations) is slightly lower than the ferromagnetic moment for pure iron and decreases slowly with increasing Cr concentration, until rapid quenching starts at 90 at. % Cr. The local iron moment in the FM alloy has a slight maxima at 6 at. % Cr after which it decreases slowly and finally vanishes for 97 at. % Cr. The local chromium moment in the FM alloy is on average antiparallel to the direction of the net magnetization in the low-Cr region and up to the equimolar composition. At higher Cr concentration the average moment on Cr is very close to zero.

It is interesting to point out that the shape of the DOS for Fe-rich alloys in the DLM state is quite similar to the canonical *d*-band shape for the more close packed fcc lattice. As a matter of fact, this may explain the big energy difference between the FM and the DLM state in the bcc Fe and Fe-rich alloys, which is of the same order as the energy difference between the FM bcc Fe and the low-spin FM fcc Fe.[15] Because the net magnetic moment rapidly decreases with increasing Cr concentration, the similarity between the DLM and fcc DOS becomes less pronounced, and the energy of the DLM state approaches that of the FM state, while the fcc-bcc energy difference increases.

V. CONCLUSIONS

The ferromagnetic bcc Fe-Cr alloy exhibits an anomalous stability for compositions around 6–9 at. % Cr. The stability is apparent in the mixing enthalpy, which is negative in this region but not for alloys of higher chromium content. The variation of the mixing enthalpy is consistently predicted by two different density functional theory methods, EMTO-CPA and PAW-SQS. The density of states at low Cr concentrations show that the states at the back slope of the antibonding peak in the spin-up channel near the Fermi level are depopulated for these compositions, while the rest of the DOS mostly retain their canonical shapes.

For more concentrated alloys the canonical shape of the band structure for the ferromagnetic density of states in the spin-up channel is smeared out as the antibonding peak is forced through the Fermi level. This is energetically unfavorable, as indicated by the positive sign of the mixing energy, and may catalyze the change of the crystal structure and a phase transition.

Furthermore, the large variation in the concentration dependence of the spin-up density of states at the Fermi level is consistently causing an inverse variation in the curvature of the mixing enthalpy, leading to a prediction of the limit for spinodal decomposition at 16 at. % Cr, in excellent agreement with experiments.

In the case of the paramagnetic alloy, which is modeled by the disordered local moments model, the behavior of the DOS is very different, and the calculated mixing enthalpy is positive for all Cr concentrations, in good agreement with experiments. For DLM alloys with high iron content, the electron occupancy at the Fermi level is higher than that of a ferromagnetic alloy and consequently the energy for the DLM alloy is higher.

ACKNOWLEDGMENTS

P.O. and I.A.A. would like to thank the Swedish Research Council (VR) and the Swedish Foundation for Strategic Research (SSF) for financial support. The Swedish National Allocations Committee and the High Performance Computing Center North are acknowledged for the generous use of supercomputing facilities.

[1] A. Koyama, A. Hishinuma, D. S. Gelles, R. L. Klueh, W. Dietz, and K. Ehrlich, J. Nucl. Mater. **233-237**, 138 (1996).
[2] E. A. Little and D. A. Stow, J. Nucl. Mater. **87**, 25 (1979).
[3] S. I. Porollo, A. M. Dvoriashin, A. N. Vorobyev, and Yu. V. Konobeev, J. Nucl. Mater. **256**, 247 (1998).
[4] F. Garner, M. B. Toloczko, and B. H. Sencer, J. Nucl. Mater. **276**, 123 (2000).
[5] R. Hultgren, P. D. Desai, D. T. Hawkins, M. Gleiser, and K. K. Kelley, *Selected Values of the Thermodynamic Properties of Binary Alloys* (American Society for Metals, Metals Park, Ohio, 1973).
[6] I. Mirebeau, M. Hennion, and G. Parette, Phys. Rev. Lett. **53**, 687 (1984).
[7] H. Kuwano and Y. Hamaguchi, J. Nucl. Mater. **155-157**, 1071 (1988).
[8] R. M. Fischer, E. J. Dulis, and K. G. Carroll, Trans. AIME **197**, 690 (1953).
[9] L. Reinhard, J. L. Robertson, S. C. Moss, G. E. Ice, P. Zschack, and C. J. Sparks, Phys. Rev. B **45**, 2662 (1992).
[10] V. Heine and J. H. Sampson, J. Phys. F: Met. Phys. **13**, 2155 (1983) and references wherein.
[11] F. Ducastelle, *Order and Phase Stability in Alloys* (North-Holland, Amsterdam, 1991).
[12] P. E. A. Turchi, L. Reinhard, and G. M. Stocks, Phys. Rev. B **50**, 15542 (1994).
[13] M. Hennion, J. Phys. F: Met. Phys. **13**, 2351 (1983).
[14] E. G. Moroni and T. Jarlborg, Phys. Rev. B **47**, 3255 (1993).
[15] P. Olsson, I. A. Abrikosov, L. Vitos, and J. Wallenius, J. Nucl. Mater. **321**, 84 (2003).
[16] H. Akai and P. H. Dederichs, Phys. Rev. B **47**, 8739 (1993).

[17] C. Jiang, C. Wolverton, J. Sofo, L.-Q. Chen, and Z.-K. Liu, Phys. Rev. B **69**, 214202 (2004).
[18] L. Vitos, I. A. Abrikosov, and B. Johansson, Phys. Rev. Lett. **87**, 156401 (2001).
[19] P. E. Blöchl, Phys. Rev. B **50**, 17953 (1994).
[20] G. Kresse and J. Hafner, Phys. Rev. B **47**, R558 (1993).
[21] G. Kresse and J. Hafner, Phys. Rev. B **49**, 14251 (1994).
[22] G. Kresse and J. Furthmüller, Comput. Mater. Sci. **6**, 15 (1996).
[23] P. Hohenberg and W. Kohn, Phys. Rev. **136**, 864 (1964).
[24] J. P. Perdew, *Electronic Structure of Solids* (Akademie Verlag, Berlin, 1991); J. P. Perdew and Y. Wang, Phys. Rev. B **45**, 13244 (1992).
[25] O. K. Andersen, O. Jespen, and G. Krier, in *Lectures on Methods of Electronic Structure Calculations*, edited by V. Kumar, O. K. Andersen, and A. Mookerjee (World Scientific Publishing, Singapore, 1994), pp. 63–124.
[26] O. K. Andersen, C. Arcangeli, R. W. Tank, T. Saha-Dasgupta, G. Krier, O. Jespen, and I. Dasgupta, *MRS Symposia Proceedings*, No. 491 (Materials Research Society, Pittsburgh, 1998), pp. 3–34.
[27] O. K. Andersen and T. Saha-Dasgupta, Phys. Rev. B **62**, R16219 (2000).
[28] L. Vitos, H. L. Skriver, B. Johansson, and J. Kollr, Comput. Mater. Sci. **18**, 24 (2000).
[29] L. Vitos, Phys. Rev. B **64**, 014107 (2001).
[30] B. L. Györffy, Phys. Rev. B **5**, 2382 (1972).
[31] J. S. Faulkner, Prog. Mater. Sci. **27**, 1 (1982).
[32] I. A. Abrikosov and H. L. Skriver, Phys. Rev. B **47**, 16532 (1993).
[33] I. A. Abrikosov and B. Johansson, Phys. Rev. B **57**, 14164 (1998).
[34] A. E. Kissavos, S. I. Simak, P. Olsson, L. Vitos, and I. A. Abrikosov, Comput. Mater. Sci. **35**, 1 (2006).
[35] N. I. Kulikov and C. Demangeat, Phys. Rev. B **55**, 3533 (1997).
[36] A. A. Mirzoev, M. M. Yalalov, and D. A. Mirzaev, Phys. Met. Metallogr. **97**, 4336 (2004).
[37] R. Hafner, D. Spisak, R. Lorenz, and J. Hafner, Phys. Rev. B **65**, 184432 (2002).
[38] H. J. Monkhorst and J. D. Pack, Phys. Rev. B **13**, 5188 (1976).
[39] C. Domain and C. S. Becquart, Phys. Rev. B **65**, 024103 (2002).
[40] C. Domain, P. Olsson, and J. Wallenius (unpublished).
[41] A. Zunger, S.-H. Wei, L. G. Ferreira, and J. E. Bernard, Phys. Rev. Lett. **65**, 353 (1990).
[42] S. I. Simak (private communication).
[43] P. A. Korzhavyi, B. Sundman, M. Selleby, and B. Johansson, Mater. Res. Soc. Symp. Proc. **842**, S4.10.1 (2005).
[44] E. Fawcett, H. L. Alberts, V. Yu. Galkin, D. R. Noakes, and J. V. Yakhmi, Rev. Mod. Phys. **66**, 25 (1994).
[45] P. G. Evans, E. D. Isaacs, G. Aeppli, Z. Cai, and B. Lai, Science **295**, 1042 (2002).
[46] W. B. Pearson, *A Handbook of Lattice Spacings and Structures of Metals and Alloys* (Pergamon Press, London, 1958).
[47] H. W. King, Science **1**, 808 (1966).
[48] I. A. Abrikosov, S. I. Simak, B. Johansson, A. V. Ruban, and H. L. Skriver, Phys. Rev. B **56**, 9319 (1997).
[49] Z. W. Lu, S.-H. Wei, and A. Zunger, Phys. Rev. B **44**, 3387 (1991).
[50] Z. W. Lu, S.-H. Wei, and A. Zunger, Phys. Rev. B **45**, 10314 (1992).
[51] W. A. Dench, Trans. Faraday Soc. **59**, 1279 (1962).
[52] R. Hafner, D. Spisak, R. Lorenz, and J. Hafner, J. Phys.: Condens. Matter **202**, 44 (2002).
[53] S. Ghosh, B. Sanyal, C. B. Chaudhuri, and A. Mookerjee, Eur. Phys. J. B **23**, 455 (2001).
[54] C. Kittel, *Introduction to Solid State Physics* (Wiley, New York, 1958).
[55] H. Jones, J. Phys. Radium **23**, 637 (1962).
[56] T. B. Massalski and U. Mizutani, Prog. Mater. Sci. **22**, 151 (1978).
[57] E. A. Smirnova, P. A. Korzhavyi, Yu. Kh. Vekilov, B. Johansson, and I. A. Abrikosov, Phys. Rev. B **64**, 020101(R) (2001).
[58] E. A. Smirnova, P. A. Korzhavyi, Yu. Kh. Vekilov, B. Johansson, and I. A. Abrikosov, Eur. Phys. J. B **30**, 57 (2002).
[59] H. Jones, Proc. R. Soc. London, Ser. A **144**, 225 (1934).
[60] J. Cieślak, S. M. Dubiel, and B. Sepiol, J. Phys.: Condens. Matter **12**, 6709 (2000).